# Search for invisible decays of the Higgs boson produced at the CEPC*

Yuhang Tan(谭雨航)[1,2] Xin Shi(史欣)[1,3;1)] Ryuta Kiuchi[1,3] Manqi Ruan(阮曼奇)[1] Maoqiang Jing(荆茂强)[1,2]
Dan Yu(于丹)[1] Kaili Zhang(张凯栗)[1,2] Xinchou Lou(娄辛丑)[1,2,3,4] Xin Mo(莫欣)[1] Gang Li(李刚)[1]
Susmita Jyotishmati[4]

[1]Institute of High Energy Physics, Beijing 100049, China
[2]School of Physical Sciences, University of Chinese Academy of Science (UCAS), Beijing 100049, China
[3]State Key Laboratory of Particle Detection and Electronics, 19B Yuquan Road, Shijingshan District, Beijing 100049, China
[4]Department of Physics, University of Texas at Dallas, Texas 75080-3021, USA

**Abstract:** The Circular Electron Positron Collider (CEPC), proposed as a future Higgs boson factory, will operate at a center-of-mass energy of 240 GeV and will accumulate 5.6 $ab^{-1}$ of integrated luminosity in 7 years. In this study, we estimate the upper limit of BR($H \to$ inv) for three independent channels, including two leptonic channels and one hadronic channel, at the CEPC. Based on the full simulation analysis, the upper limit of BR($H \to$ inv) could reach 0.26% at the 95% confidence level. In the Stand Model (SM), the Higgs boson can only decay invisibly via $H \to ZZ^* \to \nu\bar{\nu}\nu\bar{\nu}$, so any evidence of invisible Higgs decays that exceed BR($H \to$ inv) of the SM will indicate a phenomenon that is beyond the SM (BSM). The invariant mass resolution of the visible hadronic decay system $ZH(Z \to qq, H \to$ inv) is simulated, and the physics requirement at the CEPC detector for reaching this is given.

**Keywords:** CEPC, invisible Higgs decays, upper limit, boson mass resolution

**DOI:** 10.1088/1674-1137/abb4d8

## 1 Introduction

Many pieces of cosmological evidence point towards the existence of dark matter (DM), such as rotation curves in galaxies, the masses of clusters of galaxies, and the gravitational lensing of galaxies [1, 2]. However, there is no candidate for DM in the Stand Model (SM). In collider physics, the Higgs boson might be the portal connecting the new physics, such as DM and the fourth generation neutrino, and the SM [3-5]. In this case, the DM particles, which interact weakly with ordinary matter and are completely invisible to detectors, can be observed indirectly by studying the Higgs decays. In the SM, the Higgs boson can only decay invisibly via $H \to ZZ^* \to \nu\bar{\nu}\nu\bar{\nu}$, as shown in Fig. 1, and its branching ratio (BR) is $1.06\times10^{-3}$ [6]. Therefore, any evidence of invisible Higgs decays that exceed this BR will indicate a phenomenon that is beyond the SM (BSM).

The search for the invisible decays of the Higgs boson has been performed at the Large Hadron Collider (LHC). The signature for the invisible Higgs decays at the LHC is a large missing transverse momentum recoiling against a visible system. ATLAS and CMS yielded the 95% confidence level (CL) upper limits of 26% [7] and 19% [8], respectively, for the Higgs boson invisible branching ratio (BR($H \to$ inv)). These results were obtained by the ATLAS and CMS detectors, respectively, using combined 4.7 $fb^{-1}$, 20.3 $fb^{-1}$, 36.1 $fb^{-1}$ and combined 4.9 $fb^{-1}$, 19.7 $fb^{-1}$, 38.2 $fb^{-1}$ of proton-proton collisions at the center-of-mass energy of 7 TeV, 8 TeV, and 13 TeV at the LHC. Compared with the results reported by the LHC, Higgs boson candidates can be identified using a technique known as the recoil mass method without using its decays at the Circular Electron Positron Collider (CEPC) [6]. An example of the recoil mass method is as follows: in the $e^+e^- \to ZH(Z \to f\bar{f}, H \to$ inv) channel, fermions ($f$) can be identified, and their momentum

Received 4 February 2020, Revised 21 August 2020, Published online 13 October 2020

* Supported in part by the IHEP Innovation Grant (Y4545170Y2); Chinese Academy of Science Focused Science Grant (QYZDY-SSW-SLH002); Chinese Academy of Science Special Grant for Large Scientific Projects (113111KYSB20170005) and Beijing Municipal Science & Technology Commission (Z181100004218003, Z191100007219010)

1) E-mail: shixin@ihep.ac.cn

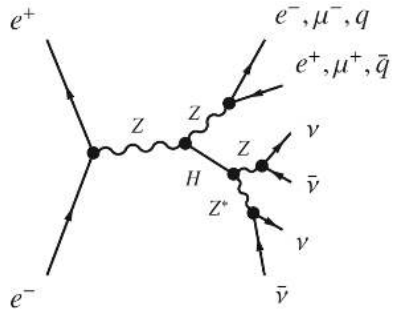


Fig. 1. Feynman diagrams of the Higgs boson's invisible decays at an electron-positron collider such as the CEPC. In the process $e^+e^- \to ZH$, the invisible decays of the Higgs boson are via $H \to ZZ^* \to \nu\bar{\nu}\nu\bar{\nu}$.

can be measured. By selecting the fermion pair from the $Z$ boson decay, the mass of the system recoiling against the fermion pair, commonly known as the recoil mass $M_{\rm recoil}$, can be calculated as

$$M_{\rm recoil} = \sqrt{(\sqrt{s} - E_{f\bar{f}})^2 - P_{f\bar{f}}^2}, \quad (1)$$

where $E_{f\bar{f}}$ and $P_{f\bar{f}}$ are the total energy and the momentum of the two fermions, respectively, and $\sqrt{s}$ is the center-of-mass energy. The $M_{\rm recoil}$ distribution is expected to exhibit a peak at the Higgs boson mass around 125 GeV for the $f\bar{f} \to ZH$ process. In this way, the properties of the Higgs boson can be measured precisely without reconstructing the Higgs boson from its decay products. Therefore, the Higgs boson production can be disentangled from its decay in a model-independent way. Moreover, the $e^+e^-$ collisions have a much lower hadronic background (Higgs boson channels form the signal) contamination compared with hadron collisions, which allows better exclusive measurements of the Higgs boson decay channels. The electron-positron Higgs factory is an essential machine for understanding the nature of the Higgs boson.

CEPC is a Higgs factory proposed by the Chinese high energy physics community. CEPC is designed for delivering a combined integrated luminosity of 5.6 ab$^{-1}$ to two detectors in 7 years. CEPC will operate at a center-of-mass energy $\sqrt{s}$ ~ 240-250 GeV, and over one million Higgs boson events will be produced during this period. Owing to the large statistics, the good beam energy spread of approximately 0.16% [9], and a novel particle flow algorithm [10], the mass and width of the Higgs boson are expected to be measured with high precision. With the SM $ZH$ production rate, the upper limit of BR($H \to$ inv) could reach 0.26% at the 95% CL, which is an expected improvement of two orders of magnitude over the results of ATLAS and CMS.

In a previous study on CEPC, the upper limit of BR($H \to$ inv) was 0.41% [6]. The previous study used the CEPC-v1 detector, whereas the CEPC-v4 detector is used in this study. The main change from CEPC-v1 to CEPC-v4 is the reduction of the solenoidal field intensity from 3.5 Tesla to 3.0 Tesla and changing the $\sqrt{s}$ of the collider from 250 GeV to 240 GeV. Moreover, the reconstruction algorithm is different in both studies. Therefore, this study does not involve the comparison of the two results.

This study performs three independent analyses corresponding to $\mu\mu H$, $eeH$, and $qqH$ channels, for estimating the upper limit on the BR($H \to$ inv) measurement at the CEPC. This paper is organized as follows. Section 2 presents a brief introduction to the CEPC detector and Monte Carlo simulations. Section 3 presents an introduction to the event selection of the three channels. A method for determining the upper limit, along with dependence of the Boson Mass Resolution (BMR), is discussed in Section 4. Section 5 lists our conclusions.

## 2 Detector design and Monte Carlo simulations

One of the physics programs at the CEPC is precision measurement of the Higgs boson properties. The CEPC detector is expected to reconstruct and identify all key physical objects, including charged leptons, photons, jets, missing energy, and missing momentum.

The CEPC-v4 [6] detector was designed using the International Large Detector (ILD) [11, 12] as a reference. The detector of CEPC-v4 is simulated using MokkaC [13] and Geant4 [14]. It is composed of a tracking system, Time-Projection-Chamber tracker (TPC), high granularity calorimeter system, solenoid that generates a 3 Tesla magnetic field, and muon detector embedded in a magnetic field return yoke. The tracking system consists of silicon vertexing and tracking detectors. The calorimetry system consists of an electromagnetic calorimeter (ECAL) and an iron scintillator for a hadronic calorimeter (HCAL).

The analysis is performed on Monte Carlo (MC) samples simulated at the CEPC-v4 detector. The Higgs boson signal and SM backgrounds at the center-of-mass energy of 240 GeV, corresponding to the overall luminosity of 5.6 ab$^{-1}$, are generated with WHIZARD1.95 [15]. The generated events are then processed with MokkaC, and an attempt is made to reconstruct every visible particle with ARBOR [10]. The cross sections of the major SM processes of the $e^+e^-$ collisions as functions of the center-of-mass energy $\sqrt{s}$ are used in the simulations, including the Higgs boson production as well as the major backgrounds, where the initial-state radiation (ISR) effect has been taken into account. The Higgs boson signal and backgrounds are processed using Geant4 based full detector simulations and reconstruction. Limited by

finite computational resources, approximately 20% of the two fermion backgrounds are used in full simulations.

All samples are grouped into signal and backgrounds, and the backgrounds are classified according to their final states. For the signal, this paper mainly focuses on the process $e^+e^- \to ZH$, which is called the "$ZH$" process. Then, $Z$ bosons decay into leptons or hadrons, and the Higgs particle decays into two $Z$ bosons, which eventually decay into four neutrinos. For the backgrounds, the major SM backgrounds are divided into 2-fermion processes and 4-fermion processes, according to the final states. The 2-fermion backgrounds are $e^+e^- \to f\bar{f}$, where $f$ refers to all lepton and quark pairs, except $t\bar{t}$. The 4-fermion backgrounds are divided into 6 types: "single_z," "single_w," "szorsw," "zz," "ww," and "zzorww," which are shown in Table 1. The processes whose four final states are a pair of electrons and two other fermions, or a pair of electron neutrinos and two other fermions, are named "single_z". The "single_w" processes include one electron, one electron neutrino, and two other fermions. If a final state includes a pair of electrons and a pair of electron neutrinos simultaneously, the corresponding processes are named "szorsw". In addition to the above-mentioned backgrounds, the same four fermions in the final state can be combined into different two intermediate bosons. If the two intermediate bosons can be two $Z$ bosons, the processes are named "zz". The "ww" process is the one in which two intermediate bosons can become two $W$ bosons. If two intermediate bosons can become two $Z$ bosons or two $W$ bosons, the corresponding process is "zzorww".

Table 1. Six types of 4-fermion backgrounds.

| Type | Four final states |
|---|---|
| single_z | Two electrons, two other fermions or two electron neutrinos, and two other fermions |
| single_w | One electron, one electron neutrino, and two other fermions |
| szorsw | A pair of electrons and a pair of electron neutrinos |
| Type | Two intermediate bosons |
| zz | Two $Z$ bosons |
| ww | Two $W$ bosons |
| zzorww | Two $Z$ bosons or two $W$ bosons |

## 3 Event selection

The signal in this analysis consists of three different channels, namely $ZH(Z \to qq, H \to$ inv), $ZH(Z \to \mu\mu, H \to$ inv), and $ZH(Z \to ee, H \to$ inv). Table 2 lists detailed information about the Higgs boson decay channels. The observed upper limit on BR($H \to$ inv) at 95% CL at the CMS is 19%, and the CEPC is expected to yield more accurate results. In the event selection part, this analysis uses BR($H \to$ inv) = 10%, and the event selection is based on the distribution of the signal and backgrounds. Event selection for each channel is detailed below.

Table 2. Cross sections of the Higgs boson production at $\sqrt{s}$ = 240 GeV and number of events expected in 5.6 ab$^{-1}$.

| Process | Cross sections /fb | Expected |
|---|---|---|
| $ffH$ | 203.66 | 1140496 |
| $e^+e^-H$ | 7.04 | 39424 |
| $\mu^+\mu^-H$ | 6.77 | 37912 |
| $q\bar{q}H$ | 136.81 | 766136 |

### 3.1 $ZH(Z \to qq, H \to$ inv)

In the $ZH(Z \to qq, H \to$ inv) process, owing to the presence of quarks, many final states are expected. The event selection uses the information about all visible particles, and the distributions of the signal and backgrounds are shown in Fig. 2. The comprehensive event selections are as follows. In the $e^+e^- \to ZH(Z \to qq, H \to$ inv) process, the mass of the system recoiling against all visible particles from the $Z$ boson is $M_{\rm recoil}^{\rm visible}$, which can be calculated using Eq. (1) by replacing $E_{f\bar{f}}$, $P_{f\bar{f}}$ with $E_{\rm visible}$, $P_{\rm visible}$. $E_{\rm visible}$ and $P_{\rm visible}$ is the total energy and momentum of all visible particles. The peak of the $M_{\rm recoil}^{\rm visible}$ distribution is close to the Higgs boson mass. Considering the resolution of the detector, $M_{\rm recoil}^{\rm visible}$ is limited to (100,150) GeV, as shown in Fig. 2(a). To suppress 2-fermion backgrounds, the transverse momentum of all visible particles is required to satisfy $P_{\rm T}^{\rm visible} > 18$ GeV, as shown in Fig. 2(b), and the difference between the azimuthal angles of the two jets should be below 175°. Two jets are reconstructed from $Z$ boson decay particles. $E_{\rm visible}$ is the energy of all visible particles, which can be described as

$$E_{\rm visible} = \frac{s + M_{\rm visible}^2 - (M_{\rm recoil}^{\rm visible})^2}{2\sqrt{s}}, \quad (2)$$

where $M_{\rm recoil}^{\rm visible}$ is approximately 125 GeV, $\sqrt{s} = 240$ GeV, and the invariant mass of the visible system ($M_{\rm visible}$) is equal to the $Z$ boson mass, which is 91.2 GeV. $M_{\rm visible}$ should be limited to (85,102) GeV, as shown in Fig. 2(c). Using the values of the parameters in Eq. (2), $E_{\rm visible}$ should be near 105 GeV, as shown in Fig. 2(d). According to the equation $P_{\rm visible}^2 = E_{\rm visible}^2 - M_{\rm visible}^2$, $P_{\rm visible}$ should be near 52 GeV. Owing to the presence of quarks, the final states may include many charged particles. It is necessary to limit the number of charged particles ($N_{\rm charged}$) with energy greater than 1 GeV to be larger than 5. To suppress the backgrounds from tau particles, a dedicated tau-finding algorithm TAURUS has been developed [16]. Since the $ZH(Z \to qq, H \to$ inv) process

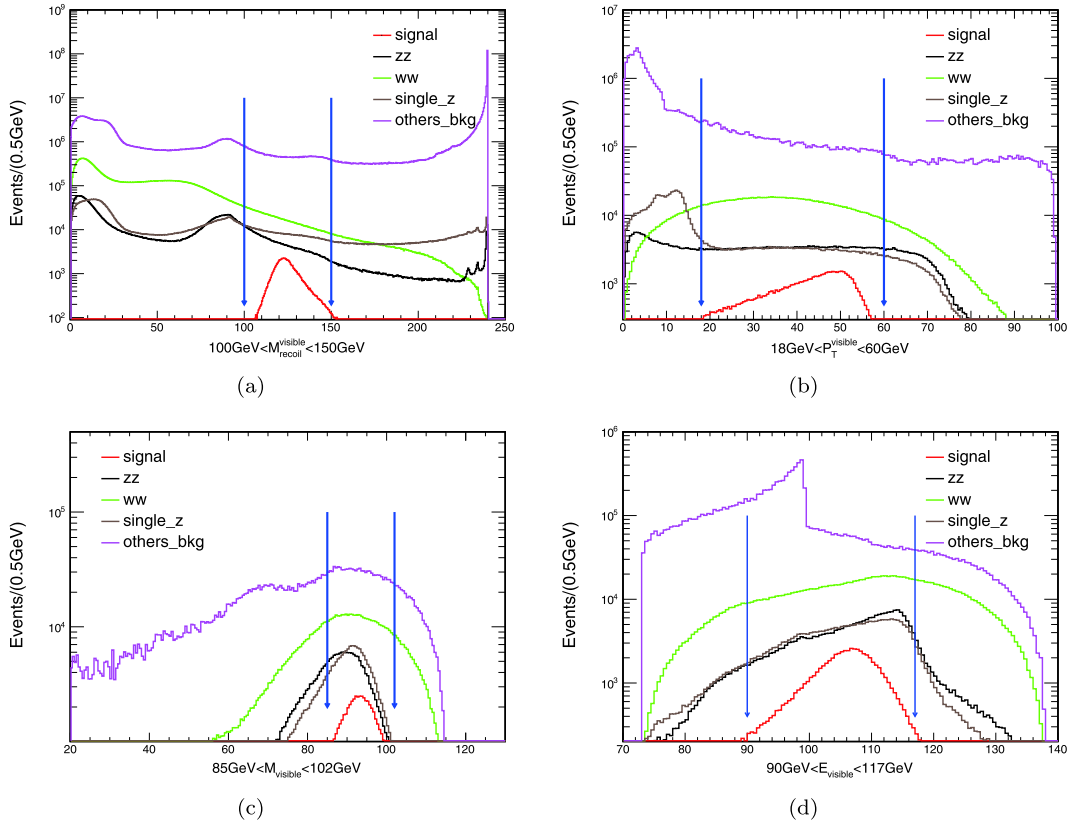


Fig. 2. (color online) The distributions of $M^{\rm visible}_{\rm recoil}$, $P^{\rm visible}_{\rm T}$, $E_{\rm visible}$, and $M_{\rm visible}$ for signal and backgrounds in the $ZH(Z\to qq, H\to {\rm inv})$ process with BR($H\to$ inv) = 10% are plotted with all cuts except the ones shown already applied in the figure and the subsequent cuts (based on Table 3). The blue arrows mark the cut ranges.

Table 3. Yields for backgrounds and $ZH(Z\to qq, H\to {\rm inv})$ signal at the CEPC, with $\sqrt{s}$ = 240 GeV, BR($H\to$ inv) = 10%, and integrated luminosity of 5.6 ab$^{-1}$.

| Process | $qqH$_inv | $2f$ | single_w | single_z | szorsw | zz | ww | zzorww | $ZH$_visible | total_bkg | Significance |
|---|---|---|---|---|---|---|---|---|---|---|---|
| Total generated | 76614 | 801152072 | 19517400 | 9072952 | 1397088 | 6389432 | 50826216 | 20440840 | 1140496 | 909936496 | 2.54 |
| 100 GeV< $M^{\rm visible}_{\rm recoil}$ <150 GeV | 73800 | 47294924 | 1388875 | 822729 | 229217 | 507567 | 1752827 | 658204 | 97387 | 52751730 | 10.16 |
| 18 GeV< $P^{\rm visible}_{\rm T}$ <60 GeV | 67115 | 9165311 | 1000762 | 269328 | 152273 | 282630 | 1294265 | 462029 | 79965 | 12706563 | 18.81 |
| 90 GeV< $E_{\rm visible}$ <117 GeV | 63912 | 5748712 | 595697 | 223049 | 92958 | 231058 | 785392 | 272518 | 33705 | 7983089 | 22.59 |
| 85 GeV< $M_{\rm visible}$ <102 GeV | 53786 | 605791 | 238191 | 148850 | 39280 | 135641 | 392277 | 113043 | 18284 | 1691357 | 41.14 |
| $\Delta\phi_{\rm dijet}$ < 175° | 51911 | 390077 | 230273 | 141494 | 38359 | 129135 | 379931 | 109735 | 17395 | 1436399 | 43.06 |
| 30 GeV< $P_{\rm visible}$ <58 GeV | 48572 | 241510 | 148607 | 69457 | 24393 | 46807 | 226883 | 74781 | 13466 | 845904 | 52.32 |
| $N_{\rm charged}>5, E_{\rm charged}>1$GeV | 47772 | 7986 | 18399 | 62990 | 6 | 43728 | 121365 | 4110 | 11699 | 270283 | 89.36 |
| $M_\tau$ <95 GeV | 46589 | 7111 | 11044 | 59815 | 1 | 41180 | 104784 | 3126 | 11111 | 238172 | 92.58 |
| Efficiency | 60.81% | 0.00% | 0.06% | 0.66% | 0.00% | 0.64% | 0.21% | 0.02% | 0.97% | 0.03% | |

may include tau particles, the mass of all tau particles ($M_\tau$) should be less than 95 GeV, for suppressing the backgrounds containing tau and quarks.

Table 3 lists the yields of signal ($qqH$_inv) and its backgrounds of the cut chain. The value of the significance [17] is used to judge the effect of the cuts. After the event selection, the signal selection efficiency is 60.81%, and the total background rejection efficiency is 99.97%. The backgrounds, which contain neutrinos and two quarks, account for 95% of the total remaining backgrounds. The compositions of these backgrounds are similar to the signal channel and are difficult to suppress further.

### 3.2 $ZH(Z\to\mu^+\mu^-, H\to {\rm inv})$ and $ZH(Z\to e^+e^-, H\to {\rm inv})$

The $ZH(Z\to\mu^+\mu^-, H\to$ inv) process and the $ZH(Z\to$

$e^+e^-, H \to$ inv) process are similar, and the two processes will be introduced together. Firstly, it is natural that only a pair of oppositely charged muons or electrons is required in the visible final states. By selecting two muons or two electrons, many related parameters can be used for background suppression. The event selections are as follows. The recoil masses of two muons ($M^{\mu^+\mu^-}_{\rm recoil}$) and two electrons ($M^{e^+e^-}_{\rm recoil}$) can be calculated using Eq. (1). The peak of $M^{\mu^+\mu^-}_{\rm recoil}$ and $M^{e^+e^-}_{\rm recoil}$ distribution should be around the Higgs boson mass 125 GeV. Considering the resolutions of muons and electrons and the distributions of signal and backgrounds as shown in Fig. 3 and Fig. 4, the recoil mass should satisfy 120 GeV$< M^{\mu^+\mu^-}_{\rm recoil} <$150 GeV or 120 GeV$< M^{e^+e^-}_{\rm recoil} <$170 GeV, and the invariant mass of two muons ($M_{\mu^+\mu^-}$) or two electrons ($M_{e^+e^-}$) is closer to the $Z$ boson mass. To suppress the 2-fermion backgrounds, the transverse momenta of the muon pair ($P_{\rm T}^{\mu^+\mu^-}$) and the electron pair ($P_{\rm T}^{e^+e^-}$) are required to be more than 12 GeV, as shown in Fig. 3(c) and Fig. 4(c). Moreover, the angle between the two muons ($\Delta\phi_{\mu^+\mu^-}$) should be under 175° or that between the two electrons ($\Delta\phi_{e^+e^-}$) should be under 176° to suppress the 2-fermion backgrounds. The visible energy ($E_{\rm visible}$), which is described in Eq. (2), is mainly the energy of two muons ($E_{\mu^+\mu^-}$) or two electrons ($E_{e^+e^-}$) from the $Z$ boson decays; the value of $E_{\rm visible}$ is approximately 105 GeV, as shown in Fig. 3(d) and Fig. 4(d). Using the approximate values of $M_{\mu^+\mu^-}$ and $E_{\mu^+\mu^-}$ in the relativistic energy-momentum relation $M^2_{\mu^+\mu^-} = E^2_{\mu^+\mu^-} - P^2_{\mu^+\mu^-}$, the value of $E_{\mu^+\mu^-}/P_{\mu^+\mu^-}$ is close to 2, similar to that of $E_{e^+e^-}/P_{e^+e^-}$.

Table 4 lists the yields for the $\mu\mu H$_inv signal and its backgrounds. The remaining backgrounds containing two muons and two neutrinos account for 61% of the total backgrounds. These backgrounds have similar topology as the signal which is difficult to suppress further. The remaining backgrounds containing the muon, tau, and two neutrinos account for 38% of the total backgrounds. The algorithm TAURUS does not increase the significance of the $\mu\mu H$_inv signal.

Table 5 lists the yields for the $eeH$_inv signal and its backgrounds at the CEPC. The cut Vertex$_\tau$ <0.0011, which is the position of the decay vertex, changes the value of significance from 10.91 to 13.79. Since the signal channel does not contain tau, the Vertex$_\tau$ of the signal channel is much smaller than the backgrounds from tau. The final states of the remaining backgrounds, which are composed of two electrons and two neutrinos, account for 70% of the total background. These back-

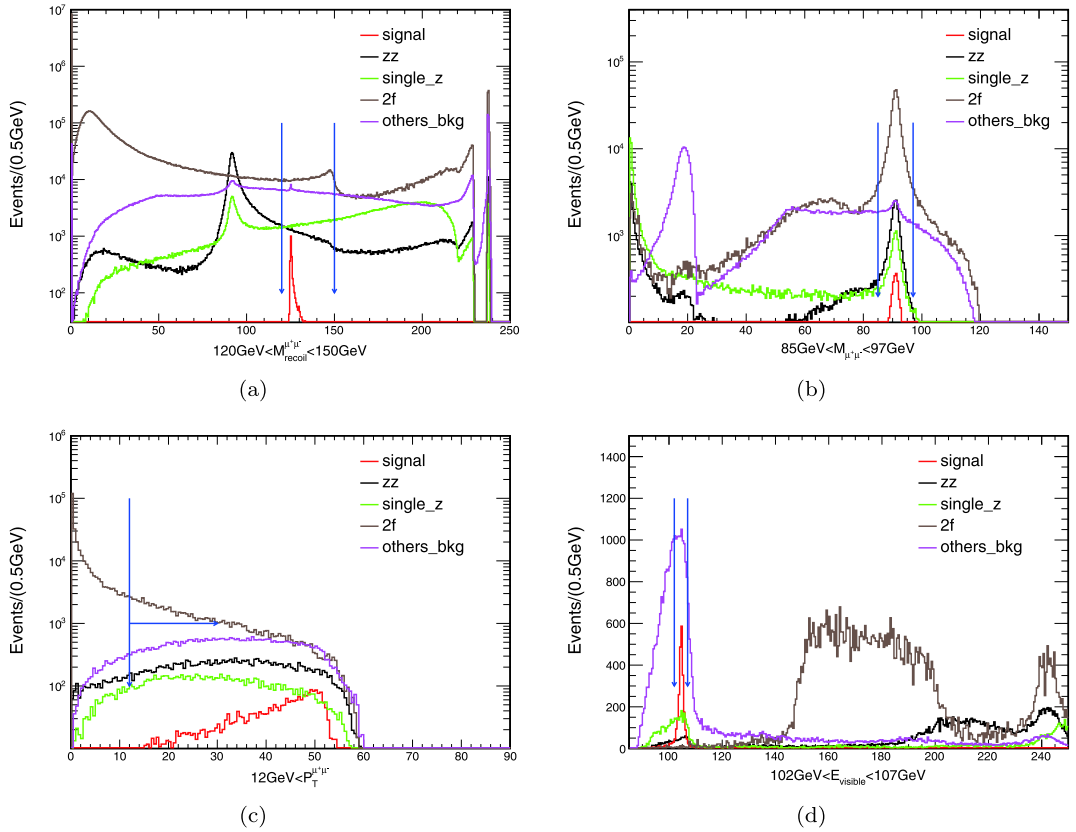


Fig. 3. (color online) The distributions of $M^{\mu^+\mu^-}_{\rm recoil}$, $P_{\rm T}^{\mu^+\mu^-}$, $E_{\rm visible}$, and $M_{\mu^+\mu^-}$ for signal and backgrounds in the $ZH(Z \to \mu^+\mu^-, H \to$ inv) process with BR($H \to$ inv) = 10% are plotted with all cuts except the ones shown already applied in the figure and the subsequent cuts (based on Table 4). The blue arrows mark the cut ranges.

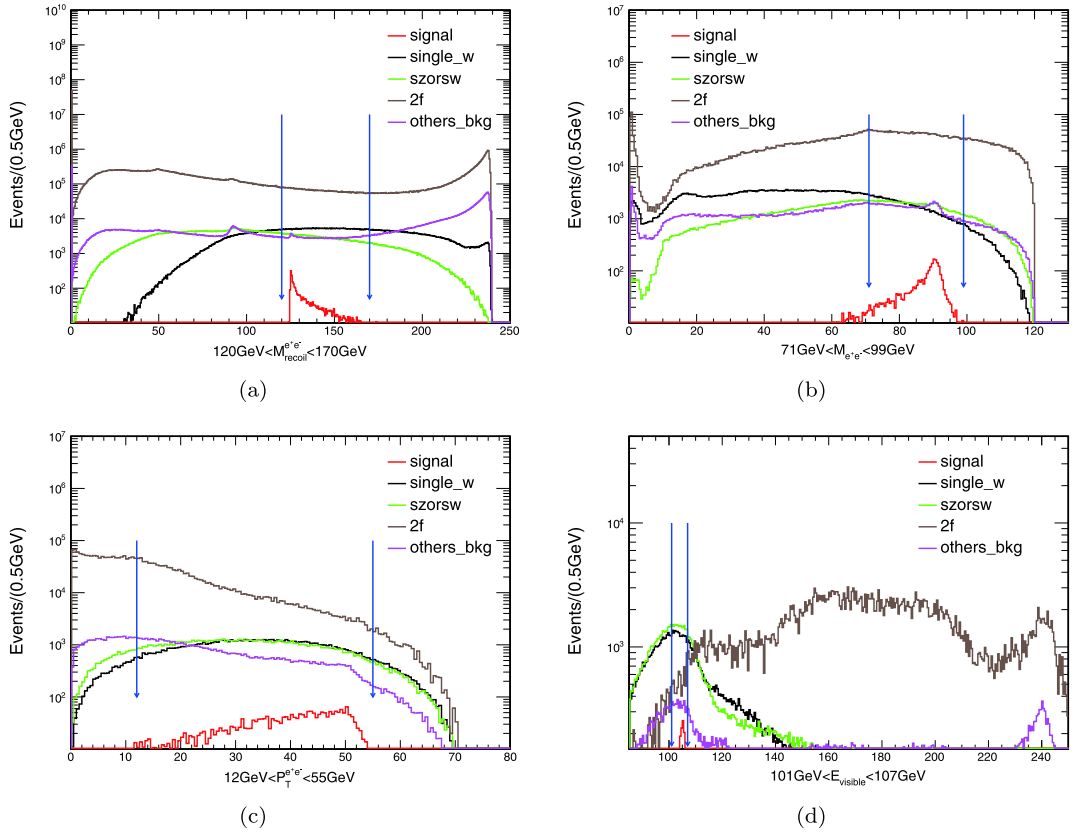


Fig. 4. (color online) The distributions of $M^{e^+e^-}_{\rm recoil}$, $P^{e^+e^-}_{\rm T}$, $E_{\rm visible}$, and $M_{e^+e^-}$ for signal and backgrounds in the $ZH(Z\to e^+e^-, H\to \text{inv})$ process with BR($H\to$ inv) = 10% are plotted with all cuts except the ones shown already applied in the figure and the subsequent cuts (based on Table 5). The blue arrows mark the cut ranges.

Table 4. Yields for backgrounds and $ZH(Z\to\mu^+\mu^-, H\to \text{inv})$ signal at the CEPC, with $\sqrt{s}$ = 240 GeV, BR($H\to$ inv) = 10% and integrated luminosity of 5.6 ab$^{-1}$.

| Process | $\mu\mu H$_inv | $2f$ | single_w | single_z | szorsw | zz | ww | zzorww | $ZH$ | total_bkg | Significance |
|---|---|---|---|---|---|---|---|---|---|---|---|
| Total generated | 3791 | 801152072 | 19517400 | 9072952 | 1397088 | 6389432 | 50826216 | 20440840 | 1140496 | 909936496 | 0.13 |
| $N_{\mu^+}=1, N_{\mu^-}=1$ | 3370 | 22737312 | 36123 | 723402 | 0 | 702045 | 1255617 | 1223596 | 59978 | 26738073 | 0.65 |
| 120 GeV< $M^{\mu^+\mu^-}_{\rm recoil}$ <150 GeV | 3286 | 652655 | 24 | 100435 | 0 | 62463 | 250819 | 112143 | 5708 | 1184247 | 3.02 |
| 85 GeV< $M_{\mu^+\mu^-}$ <97 GeV | 2791 | 381056 | 0 | 10739 | 0 | 20857 | 16720 | 24419 | 4493 | 458284 | 4.12 |
| 12 GeV< $P^{\mu^+\mu^-}_{\rm T}$ | 2705 | 92200 | 0 | 9483 | 0 | 18257 | 15906 | 21063 | 4331 | 161240 | 6.72 |
| $\Delta\phi_{\mu^+\mu^-}<175°$ | 2598 | 72197 | 0 | 8894 | 0 | 17029 | 14769 | 20231 | 4142 | 137262 | 6.99 |
| 102 GeV< $E_{\rm visible}$ <107 GeV | 2273 | 62 | 0 | 1456 | 0 | 484 | 4379 | 5435 | 10 | 11826 | 20.28 |
| $\frac{E_{\mu^+\mu^-}}{P_{\mu^+\mu^-}}<2.4$ | 2243 | 27 | 0 | 1344 | 0 | 440 | 3502 | 4090 | 6 | 9409 | 22.29 |
| Efficiency | 59.17% | 0.00% | 0.00% | 0.01% | 0.00% | 0.01% | 0.01% | 0.02% | 0.00% | 0.00% | |

grounds are the same as the final particles of the signal channel. The final particles of the remaining backgrounds containing tau, electron, and two neutrinos account for 23% of the total background, and the information about tau particles cannot further suppress these backgrounds. In conclusion, the tau-finding algorithm TAURUS can improve the significance of the Higgs invisible decays to a certain extent, but it cannot completely suppress the backgrounds containing tau.

## 4 Results for the upper limit and the boson mass resolution (BMR)

After the event selections, the 95% CL upper limit of BR($H\to$ inv) is computed within the CL$_s$ formalism, us-

Table 5. Yields for backgrounds and $ZH(Z\to e^+e^-, H\to \text{inv})$ signal at the CEPC, with $\sqrt{s}$ = 240 GeV, BR($H\to$ inv) = 10%, and integrated luminosity of 5.6 ab$^{-1}$.

| Process | $eeH$_inv | 2f | single_w | single_z | szorsw | zz | ww | zzorww | ZH | total_bkg | Significance |
|---|---|---|---|---|---|---|---|---|---|---|---|
| Total generated | 3942 | 801152072 | 19517400 | 9072952 | 1397088 | 6389432 | 50826216 | 20440840 | 1140496 | 909936496 | 0.13 |
| $N_{e^+}=1, N_{e^-}=1$ | 3472 | 120476492 | 1286971 | 1945217 | 1161098 | 134637 | 796860 | 292694 | 117024 | 126210993 | 0.31 |
| 120 GeV< $M^{e^+e^-}_{\text{recoil}}$ <170 GeV | 3179 | 6469896 | 515411 | 226357 | 288321 | 4901 | 12836 | 34015 | 12443 | 7564180 | 1.16 |
| 71 GeV< $M_{e^+e^-}$ < 99GeV | 2617 | 2415241 | 98434 | 69803 | 105255 | 453 | 926 | 10853 | 9153 | 2710118 | 1.59 |
| 12 GeV< $P^{e^+e^-}_{\text{T}}$ <55 GeV | 2511 | 1351168 | 87124 | 45901 | 91180 | 352 | 788 | 9396 | 8774 | 1594683 | 1.99 |
| $\Delta\phi_{e^+e^-}$ < 176° | 2397 | 462573 | 81317 | 37220 | 87409 | 208 | 712 | 8613 | 8456 | 686508 | 2.89 |
| 101 GeV< $E_{\text{visible}}$ <107 GeV | 1614 | 6555 | 15198 | 2820 | 17583 | 12 | 54 | 1175 | 47 | 43444 | 7.70 |
| 1.8 < $\frac{E_{e^+e^-}}{P_{e^+e^-}}$ < 2.4 | 1455 | 1423 | 6634 | 1127 | 7685 | 4 | 17 | 393 | 23 | 17306 | 10.91 |
| Vertex$_{\text{r}}$ <0.0011 | 1393 | 323 | 2436 | 926 | 5967 | 1 | 7 | 86 | 9 | 9755 | 13.79 |
| Efficiency | 35.34% | 0.00% | 0.01% | 0.01% | 0.43% | 0.00% | 0.00% | 0.00% | 0.00% | 0.00% | |

ing the profile likelihood ratio as a test statistic [18], in which systematic uncertainties are ignored. The likelihood ratio method uses $\mu$S+B, where $\mu$ is the signal strength, S is the signal, and B is the background. First, the signal and background samples are fitted to obtain their distribution functions, which are used for generating Asimov data. The Asimov data provide a simple method for obtaining the median experiment sensitivity of the measurement as well as fluctuations around this expectation. Then, the test statistic distribution generated for signal+background and background-only hypotheses is constructed assuming the signal strength $\mu$, and each $\mu$ corresponds to the CL$_s$ value calculated by the ratio of the two hypothesis probabilities [19]. When the CL$_s$ value is 0.05, the $\mu$ value is its 95% CL upper limit. The corresponding negative logarithmic profile likelihood ratio $-\Delta\log(L)$ as a function of $\mu$ is shown in Fig. 5. The horizontal axis corresponding to $-\Delta\log(L)$ = 2 on the $y$-axis is approximately 95% CL interval of $\mu$.

Table 6 summarizes the expected precision of the measurement of BR($H\to$ inv) and the 95% CL upper limit on BR($H\to$ inv), for the dataset of 5.6 ab$^{-1}$. The estimated combined 95% CL upper limit of three channels is 0.26%. Any evidence of invisible Higgs decays that exceeds this value will indicate the BSM phenomenon.

The precision of the upper limit is affected by various systematic uncertainties [20], such as the luminosity, beam energy, efficiency of the object reconstruction, and acceptance of the detector. The precision of luminosity can be 0.1%, and the beam energy is expected to be better than 1 MeV, which can be ignored in experimental recoil mass measurements. For tracks within the detector acceptance and transverse momenta larger than 1 GeV, the track finding efficiency is better than 99%. These systematic uncertainties are expected to be small and will be ignored in this study.

The precision of the upper limit of BR($H\to$ inv) in

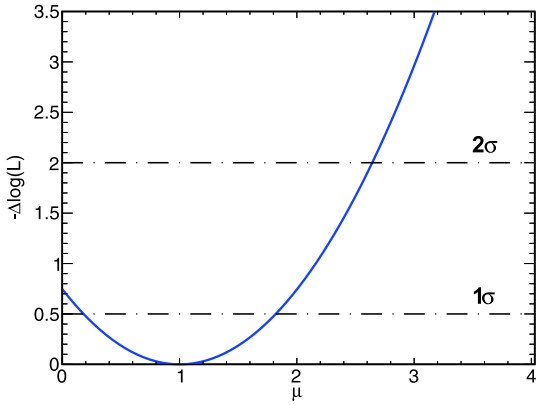


Fig. 5. (color online) The $\mu$ distribution from the likelihood profile, where the horizontal dash-dotted lines indicate the location of the approximately 68%, 95% CL interval, which corresponds to $-\Delta\log(L)$ = 0.5, 2 on the $y$-axis.

Table 6. Expected precision of the measurement of BR($H\to$ inv) and the 95% CL upper limit on BR($H\to$ inv) for the dataset 5.6 ab$^{-1}$.

| $ZH$ final states | Precision of BR($H\to$ inv)×100 (%) | Upper limit on BR($H\to$ inv) (%) |
|---|---|---|
| $Z\to e^+e^-$, $H\to$ inv | 45.37 | 1.08 |
| $Z\to \mu^+\mu^-$, $H\to$ inv | 23.57 | 0.55 |
| $Z\to q\bar{q}$, $H\to$ inv | 9.54 | 0.27 |
| Combination | 8.68 | 0.26 |

$ZH(Z\to qq, H\to$ inv) channel strongly relies on the invariant mass reconstruction of the $Z$ boson. The boson mass resolution (BMR) is defined as the visible invariant mass resolution of the $ZH(Z\to qq, H\to$ inv) event for quantifying the invariant mass reconstruction of the $Z$ boson.

The BMR of the CEPC detector can reach 3.8% using the ARBOR reconstruction algorithm [10, 21]. A fast simulation was performed for quantifying this depend-

ence. The fast simulation took into account the signal of $ZH(Z\to qq,H\to$ inv) and the main background of $ZZ(Z\to qq,Z\to$ inv) after the event selection. Fig. 6 shows the accuracy [16] of $ZH(Z\to qq,H\to$ inv) for different BMR values. For BMR values between 4% and 20%, the accuracy degrades rapidly with increasing BMR, while for BMR values below 4%, the change in the accuracy is below 0.06%. Based on the fast simulation, it can be concluded that BMR is vital and will affect the measurement precision of the $ZH(Z\to qq,H\to$ inv) channel. Therefore, the BMR value of 4% can be used as an essential reference upper bound for detector design and optimization.

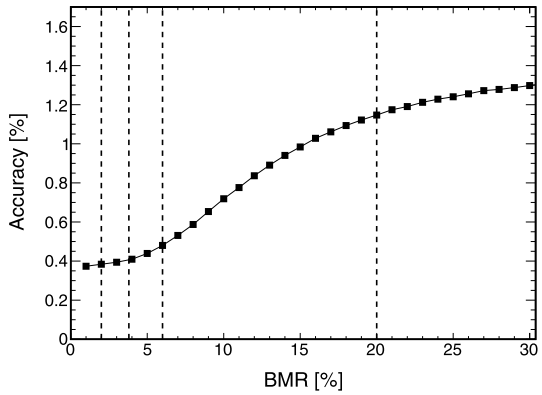


Fig. 6. Accuracy of the $qqH$ ($H\to$inv) channel vs. BMR, for the background of $ZZ(Z\to qq,Z\to$ inv). The dashed vertical lines show the accuracy at BMR is 2%, 3.8%, 6%, and 20%, assuming BR($H\to$ inv) = 10%.

## 5 Conclusion

This paper studied the measurement of the Higgs invisible decays at the CEPC. The upper limit on the Higgs invisible decays was measured using three independent channels $ZH(Z\to qq,H\to$ inv), $ZH(Z\to\mu^+\mu^-,H\to$ inv), and $ZH(Z\to e^+e^-,H\to$ inv). The combined result for the 95% CL upper limit of BR($H\to$ inv) was 0.26% for the three channels. Compared with the LHC results (26% for ATLAS and 19% for CMS), the result obtained at the CEPC is better by two orders of magnitude. Compared with the High-Luminosity LHC (HL-LHC) result for 14 TeV, which is expected to be 2.5% [22], the result obtained at the CEPC is better by one order of magnitude. The accuracy of the upper limit for the CEPC is significantly better than those for hadron colliders, because the reconstructed Higgs recoil mass spectrum at the electron-positron Higgs factories gives a very clear and distinct signature of the Higgs boson, as well as the high productivity of the Higgs bosons at the CEPC.

The CEPC result is consistent with the results for other electron-positron colliders, such as the International Linear Collider (ILC) and the Future Circular Collider (FCC-ee), for which the 95% CL upper limits on BR($H\to$ inv) were 0.26% for ILC [23] and 0.22% for FCC-ee (5 ab$^{-1}$ at 240 GeV and 0.19% by combining 365 GeV) [24]. Among these three signal channels, the $qqH$ channel yielded the best result owing to its largest number of events. The precision of the upper limit on the $qqH$ channel strongly relies on the invariant mass of the visible hadronic decay system, and BMR better than 4% provides a clear separation between the Higgs signal and the $ZZ$ background, which shall be pursued as one of the key physics requirements for designing future CEPC detectors.

*The authors would like to thank Chengdong FU and Xianghu ZHAO for providing the simulation tools and samples. We also thank Patrick Janot for a helpful discussion about FCC results.*

## References

1 G. Bertone *et al*., Rev. Mod. Phys., **90**(4): 045002 (2018)
2 D. Clowe *et al*., Astrophys. J. Lett., **648**: L109-L113 (2006)
3 A. Djouadi *et al*., Phys. Lett. B, **709**: 65-69 (2012)
4 R. E. Shrock *et al*., Phys. Lett. B, **110**: 250 (1982)
5 K. Belotsky *et al*., Phys. Rev. D, **68**: 054027 (2003)
6 F. An *et al*., Chin. Phys. C, **43**(4): 043002 (2019)
7 M. Aaboud *et al*., Phys. Rev. Lett., **122**(23): 231801 (2019)
8 A. M Sirunyan *et al*., Phys. Lett. B, **793**: 520-551 (2019)
9 Z. Chen *et al*., Chin. Phys. C, **41**(2): 023003 (2017)
10 M. Ruan *et al*., Arbor, a new approach of the Particle Flow Algorithm. In *International Conference on Calorimetry for the High Energy Frontier*, pages 316-324, 2013
11 T. Abe *et al*., The International Large Detector: Letter of Intent. 2010
12 H. Abramowicz *et al*., *The International Linear Collider Technical Design Report - Volume 4: Detectors*. Technical report, 2013
13 C. Fu., Full simulation software at CEPC. http://cepcdoc.ihep.ac.cn/DocDB/0001/000167/002/CEPCNoteCover.pdf, 2019
14 L. Sartini *et al*., Nucl. Instrum. Meth. A, (2010)
15 W. Kilian *et al*., Eur. Phys. J. C, **71**: 1742 (2011)
16 D. Yu *et al*., Eur. Phys. J. C, **80**(1): 7 (2020)
17 G. Cowan, Discovery sensitivity for a counting experiment with background uncertainty. 2020
18 G. Cowan *et al.*, Eur. Phys. J. C, **71**: 1554, 2011, [Erratum: Eur. Phys. J. C, **73**: 2501 (2013)]
19 The ATLAS, CMS Collaborations, and the LHC Higgs Combination Group, Procedure for the LHC Higgs boson search combination in Summer 2011. Technical Report CMS-NOTE-2011-005. ATL-PHYS-PUB-2011-11, CERN, Geneva, 2011
20 CEPC Study Group, CEPC Conceptual Design Report: Volume 2 - Physics & Detector. 2018
21 H. Zhao *et al*., Chin. Phys. C, **43**(2): 023001 (2019)
22 M. Cepeda *et al*., CERN Yellow Rep. Monogr, **7**: 221-584 (2019)
23 A. Ishikawa, Search for invisible decays of the Higgs boson at the ILC, *PoS*, LeptonPhoton2019: 147, 2019
24 J. de Blas *et al*., JHEP, **01**: 139 (2020)